THE JOURNAL OF PHYSICAL CHEMISTRY Letters

Letter

pubs.acs.org/JPCL

Tetracene Aggregation on Polar and Nonpolar Surfaces: Implications for Singlet Fission

Steven E. Strong and Joel D. Eaves*

Department of Chemistry and Biochemistry, University of Colorado, Boulder, Colorado 80309, United States

Supporting Information

ABSTRACT: In molecular crystals that exhibit singlet fission, quantum yields depend strongly on intermolecular configurations that control the relevant electronic couplings. Here, we explore how noncovalent interactions between molecules and surfaces stabilize intermolecular structures with strong singlet fission couplings. Using molecular dynamics simulations, we studied the aggregation patterns of tetracene molecules on a solid surface as a function of surface polarity. Even at low surface concentrations, tetracene self-assembled into nanocrystallites where about 10−20% of the clustered molecules were part of at least one herringbone structure. The herringbone structure is the native structure of crystalline tetracene, which exhibits a high singlet fission quantum yield. Increasing the polarity of the surface reduced both the amount of clustering and the relative number of herringbone configurations, but only when the dipoles on the surface were orientationally disordered. These results have implications for the application of singlet fission in dye-sensitized solar cells.

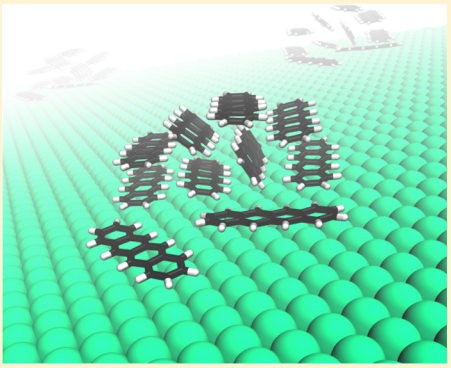

Singlet fission (SF), a process where one singlet excited state relaxes into two triplets, is a fundamentally interesting electronic process that can address an important loss mechanism in conventional single-junction solar cells.[1] In such a cell, electrons excited by the absorption of photons with energies greater than the optical gap dissipate this excess energy as heat.[2] A solar cell with both a SF chromophore and a conventional chromophore absorbs those high-energy photons and splits them into two electrons, preventing heat loss. A device using this mechanism could break the Shockley−Quiesser detailed balance limit that bounds the efficiency of single-chromophore/single-junction solar cells.[1,2] In many ways, such a device would function as a multiple-junction solar cell without the current-matching constraint.[1] A dye-sensitized solar cell (DSSC), in which both SF and conventional chromophores adsorb onto the surface of semiconducting nanoparticles, is one concrete realization of such a device that resonates closely with the work presented here.[1,3−5]

For SF to occur with high efficiency, the singlet and two triplet states must have comparable energy and be coupled sufficiently strongly.[6−10] The large exchange energy present in acene molecules satisfies the energy-matching criterion.[6,7] The electronic couplings, however, depend strongly on intermolecular geometry.[6,7,11−45] Many studies find a variety of geometries that promote SF, but these geometries depend on the molecular system.[10,12−20] While the precise intermolecular orientations that maximize SF are unknown, both calculations and experiments suggest that SF can occur with high efficiency in acenes when the molecules adopt a herringbone structure (Figure 1a).[6,7,21,23,41] Since this is the structure found in many crystalline acenes at ambient conditions, it is natural that SF was first discovered in them.[1] In a DSSC, however, the intermolecular structures of the molecules at noncrystalline densities determine the efficiency of SF. These structures depend, in complex ways, on the molecular structures of the aggregating molecules and on the interactions of those molecules with the surface.[46−49]

A large body of work, on both dimers and crystals, has manipulated the intermolecular structure of pentacene and tetracene derivatives through synthetic modifications to covalent architectures.[8,10,13,14,17,18,28,30,50,51] We pursue a complementary approach that examines how noncovalent interactions guide the self-assembly of intermolecular structures. In particular, we study how interactions with the surface promote the assembly of aggregates that can undergo SF. Experiments have found that the absorption spectrum of tetracene adsorbed to amorphous silica exhibits a splitting similar to the Davydov splitting in bulk crystalline tetracene, even at low surface concentration (1−2% of a monolayer).[49] This suggests that the structures of the adsorbed aggregates are similar to those in the bulk crystal, but this is, so far, an untested hypothesis. Our work examines this hypothesis and addresses a knowledge gap between the bulk (crystalline) and molecular (solution-phase) structural properties of acenes.

The chemical, electronic, and topological properties of a surface all play a role in aggregation.[52−55] Here, we investigate the effects of surface polarity using a model that encompasses both microscopically and macroscopically polar surfaces. A microscopically polar surface is one that is polar on atomic length scales but macroscopically nonpolar because of symmetry or disorder. Our motivations for studying the effects of surface

Received: January 21, 2015
Accepted: March 11, 2015
Published: March 11, 2015

DOI: 10.1021/acs.jpclett.5b00141
J. Phys. Chem. Lett. 2015, 6, 1209−1215

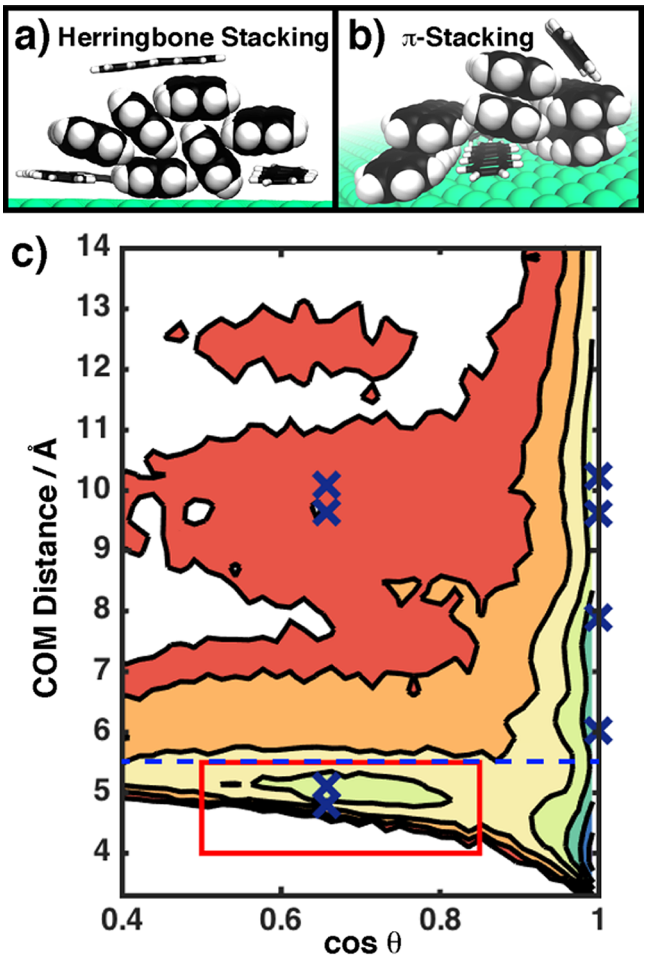

Figure 1. Snapshots from simulations of tetracene show space-filled molecules in (a) herringbone and (b) π-stacked configurations according to our geometric criteria. (c) The Helmholtz free energy density for tetracene on a nonpolar surface as a function of the center-of-mass (COM) distance between two molecules and the cosine of their stacking angle, as described in the text. The free energy does not change qualitatively as a function of surface polarity. The contours are spaced by $1k_BT$, with free energy decreasing toward the cooler colors. It is important to analyze the data in the cosine of the angle rather than in the angle itself to avoid singularities in the Jacobian.[70] The blue dashed line is the cutoff used to identify neighbors in the clustering calculation, and the red box illustrates the geometric criterion that we use to identify herringbone structures. The blue ×s indicate the minima of the free energy for the experimental structure of crystalline tetracene.[71] The red box surrounds the herringbone signatures in the crystal phase and the associated basin in the free energy for clusters. The π-stacked configurations in (b) correspond to the minimum in the free energy at cos θ = 1 and a COM distance of ~4 Å.

polarity are as follows: Recent work has found that SF is only competitive with singlet electron injection in a DSSC when a spacer layer between the chromophores and the semiconductor surface slows down electron injection.[5] Tailoring the intermolecular interactions between the substrate and the chromophores in a DSSC by adjusting the polarity of the spacer layer might offer considerable design flexibility. Surface polarity is also an important feature in materials such as amorphous silica, which was used in the experiments by Dabestani and co-workers,[49] and titanium dioxide, a semiconductor frequently used in DSSCs.[3,56] Silica has both a microscopically disordered polarity from the random orientations of the Si−O bonds at the surface and an ordered polarity from passivation by hydrogen.[57] In crystalline titanium dioxide, the most stable surfaces are not macroscopically polar,[58] even though the Ti−O bond is polar on microscopic length scales. Surface passivation can also render many nonpolar surfaces polar. For example, silicon passivated with Al_2O_3 exhibits a macroscopically polar surface.[59] Finally, during solar cell operation, space−charge regions form at the interfaces between materials, creating electric fields similar to those from a polar surface.[60,61] In this work, we use the term "surface polarity" to encompass cases in which the surface is polar on macroscopic length scales *and* those in which the surface is polar on molecular length scales but nonpolar on macroscopic ones. This differs from the usual convention that uses the term surface polarity only to describe surfaces that are macroscopically polar.[58,62]

Because tetracene is a canonical SF chromophore, we explored the aggregation patterns of tetracene molecules on surfaces as a function of surface polarity. We performed molecular dynamics simulations using the DREIDING force field for the tetracene molecules,[63] which qualitatively reproduces experimentally determined crystal structures at room temperature and pressure.[64] The results reported here used replica exchange molecular dynamics (REMD) to achieve thermal equilibration.[65] We modeled the surface by a slab of Lennard-Jones particles with point dipoles at their centers, oriented either uniformly or randomly, to mimic an ordered or disordered polar surface, respectively. We report surface polarity in units of the magnitude of the dipole moment of the surface particles. All simulations were done with the LAMMPS package,[66] and all simulation snapshots (Figure 1a,b) were generated with the VMD and Tachyon packages.[67,68] Details of the simulations appear in the Supporting Information.

Even at low concentrations (5% of a monolayer), between 40 and 75% of the molecules were in clusters of size two or larger (Figure 2a). Of those molecules in clusters, between 10 and 20% of them were in at least one herringbone configuration (Figure 2a). The fraction of molecules in clusters was independent of polarity on ordered polar surfaces (Figure 2b). On disordered polar surfaces, however, the polarity had a qualitative impact on both the clustering statistics (Figures 2a and 3) and the number of herringbone structures observed in clusters (Figure 2a). On these disordered polar surfaces, diffusion constants decreased exponentially with polarity (Figure 4), implying that energetic roughness on a disordered polar surface provides some degree of trapping.

Snapshots from simulations show both herringbone structures and π-stacked structures, in which the molecules lie flat on one another (Figure 1a,b). While the experimental evidence supporting the notion that the herringbone configuration promotes efficient SF is overwhelming, some calculations have predicted that the π-stacked structures also promote SF.[6,7,16,20,45] The stacking angle, defined as the angle between the vectors normal to the molecular planes, distinguishes these two configurations. The stacking angle alone cannot, however, unambiguously identify either configuration. It does not resolve rotations about the normal axis of either molecule, nor does it resolve a slip along the long or short molecular axis. The molecular center-of-mass (COM) distance, in conjunction with the stacking angle, helps resolve these ambiguities. We constructed a Helmholtz free energy surface as a function of the COM distance, R_{COM}, and the cosine of the stacking angle, cos θ, by measuring the probability of observing a given configuration, $P(R_{COM}, \cos\theta)$, through histogramming. Ignoring

DOI: 10.1021/acs.jpclett.5b00141
J. Phys. Chem. Lett. 2015, 6, 1209−1215

physically irrelevant constants, the Helmholtz free energy density is

$$F(R_{COM}, \cos\theta) = -k_B T \ln\left(\frac{P(R_{COM}, \cos\theta)}{R_{COM}^2}\right)$$

where T is the absolute temperature, 296 K, and k_B is Boltzmann's constant.[69] We normalize by R_{COM}^2 so that the free energy density reduces to the potential of mean force in three dimensions when $\cos\theta$ is integrated out of $P(R_{COM}, \cos\theta)$.[69] Figure 1c shows the free energy surface along with the expected minima corresponding to the experimental crystal structure.

Figure 1c also shows the geometric criteria that we used to identify clusters and to assign intermolecular herringbone structures. To quantify clustering, we defined a cluster as a group of molecules connected by neighbors for which R_{COM} was less than 5.5 Å (blue dashed line in Figure 1c). This definition includes both the first and second peaks in the radial distribution function of the aggregates. The first peak corresponds to π-stacked and similar configurations, which are not present in the crystal, while the second corresponds to the herringbone configuration. We defined a herringbone configuration as a pair of molecules for which R_{COM} was less than 5.5 Å and $\cos\theta$ was between 0.5 and 0.85. The red box in Figure 1c shows this region. We defined p_H as the conditional probability that a molecule was in a herringbone configuration with at least one neighbor *provided* that it was also in a cluster. We computed p_H by averaging the number of molecules in at least one herringbone configuration and dividing by the total number of clustered molecules.

Figure 2a shows that both the fraction of molecules in clusters and p_H decreased with increasing surface polarity, but only when the dipoles were oriented randomly. When the dipoles were all aligned perpendicular to the surface, clustering was independent of surface polarity (Figure 2b). To investigate the effects of surface concentration and finite system size, we performed simulations with a fixed number of molecules on both a large and a small slab: low and high surface concentration, respectively. From equilibrium arguments, one would expect the fraction of clustered molecules to scale inversely with the area for a fixed number of molecules, so the fraction of clustered molecules multiplied by the surface area should be the same for any size slab. This was true, except on the small slab at high polarities, where the results saturated to a minimum clustering fraction for that slab size (Figure 2b).

To gain deeper insight into how polarity impacts clustering, we computed probability distribution functions of cluster size for various surface polarities. Figure 3 shows these distributions and hints at some degree of cooperativity during clustering. To model cooperativity, we considered a null hypothesis of noncooperativity. In the noncooperative picture, all molecules in clusters of all sizes behave in exactly the same way; each molecule in the cluster can dissociate from the cluster at any time, with a rate k_d, and any molecule in the cluster can associate with a new molecule at any time, with a rate k_a. Ignoring events in which larger pieces (dimers, trimers, etc.) associate or dissociate simultaneously, which should be rare at the low concentrations studied here, clusters can only change size by one molecule at a time. For $n > 1$, the following master equation describes this scenario

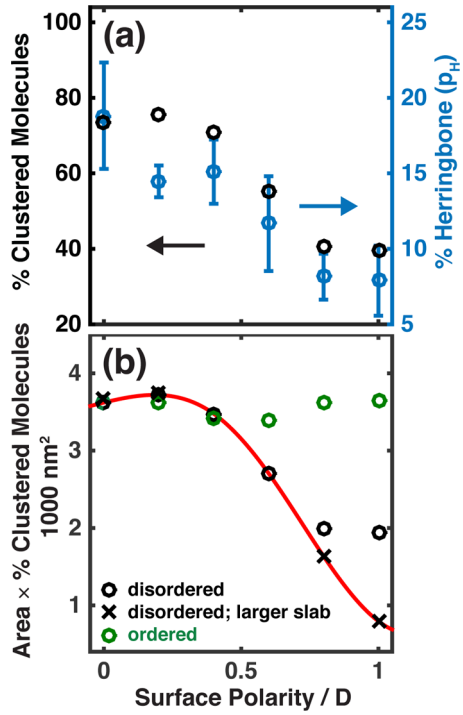

Figure 2. (a; left axis) The fraction of clustered molecules decreased as a function of surface polarity when the orientations of the dipoles on the surface were disordered. (a; right axis) Of molecules in clusters, the fraction in herringbone structures also decreased as a function of surface polarity. (b) The fraction of clustered molecules multiplied by the surface area for both random (black) and uniform dipoles (green) in simulations with a fixed number of molecules on a small slab (○) and a large slab (×). Multiplying the fraction of clustered molecules by the surface area should put the large and small slab simulations on the same curve. The red line is a guide for the eye that follows this curve. The data for the small slab do not fall on the red curve for polarities larger than 0.6 D because the size of the slab limits the minimum clustering fraction. The fraction of molecules in a cluster did not depend on the surface polarity when dipoles were uniformly oriented either parallel or perpendicular to the slab (green ○). Note that for a nonpolar surface (0 D), the distinction between ordered and disordered polarity is meaningless. All absolute error bars are less than ±10% or 500 nm².

$$\frac{dP_n(t)}{dt} = k_a(n-1)P_{n-1}(t) + k_d(n+1)P_{n+1}(t) - (k_d + k_a)nP_n(t)$$

where $P_n(t)$ is the probability of finding a cluster of n molecules at time t. At steady state, $dP_n(t)/dt = 0$, we find the equilibrium clustering probabilities, $\{P_n\}$, by solving the recurrence relation

$$K(n-1)P_{n-1} + (n+1)P_{n+1} - (1+K)nP_n = 0$$

where $K \equiv k_a/k_d$ is the equilibrium constant. The solution can be found using the ansatz $nP_n = z^n$, with appropriate boundary conditions, and is

$$P_n = \frac{1-K^n}{n}\left(\frac{P_1}{1-K}\right)$$

While the numerator tends to unity exponentially fast, P_n goes as a power law, n^{-1}, for asymptotically large n. Our data decay faster than the n^{-1} expectation from the noncooperative model at all polarities, but especially for polarities above 0.4 D where the decay law is closer to n^{-3}. This could mean that clustering becomes increasingly anticooperative as surface polarity

DOI: 10.1021/acs.jpclett.5b00141
J. Phys. Chem. Lett. 2015, 6, 1209−1215

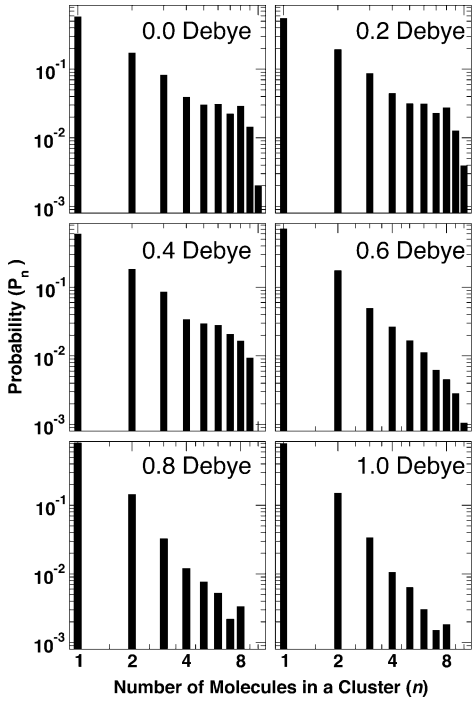

Figure 3. The probability of observing a cluster containing n molecules for various values of polarity on a disordered surface. Large cluster sizes occur with a much lower frequency than a noncooperative model would predict, especially for polarities above 0.4 D. To account for this observation, we explore two mechanisms: anticooperative cluster growth and monomer trapping to the surface.

increases; that is, the larger a cluster grows, the more it resists growth. But there is an alternate scenario where the surface plays a pivotal role. The fluctuations in polarity on disordered surfaces give molecules opportunities to find pockets on the surface to which they strongly attract, effectively trapping them and making it more difficult for them to join clusters.

To distinguish between these two mechanisms, we studied the hypothesis that trapping inhibited clustering by calculating the diffusion constant of one molecule on a surface. The two-dimensional diffusion constant, D_{2d}, was computed from the mean-squared displacement of a single tetracene molecule's COM projected onto the plane of the surface. The mean-squared displacement was computed as an average over many trajectories and realizations of the disorder. D_{2d} decreased exponentially with polarity on a disordered surface (Figure 4), confirming that the tetracene molecules adhered more strongly to the surface at higher polarities.

To cast this observation in the theoretical framework of diffusion in disordered media, one must translate the dependence of D_{2d} on the polarity to its dependence on the potential energy. The fluctuations in the potential are more drastic when the randomly oriented dipoles have larger magnitudes, so the variance of the potential fluctuations should scale with the polarity. There are, unfortunately, few theories that relate the quenched disorder of a potential to the renormalization of the diffusion constant without resorting to the phenomenology of continuous time random walks.[72,73] In one dimension, Zwanzig showed that the diffusion constant depends exponentially on the variance of the potential energy when the fluctuations are drawn from a Gaussian distribution.[74] To see if our data fit this trend, we computed the variance of the interaction energy between a tetracene molecule and the surface. While the variance did

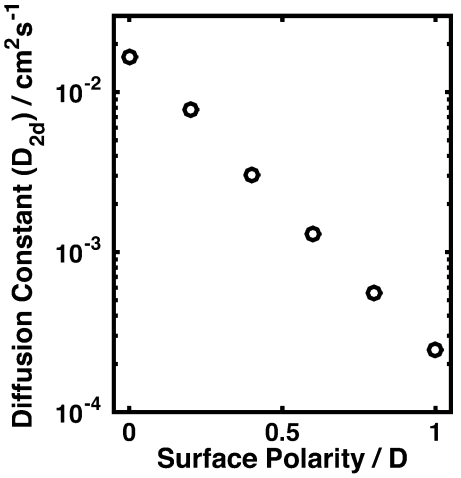

Figure 4. Diffusion constants decreased exponentially with polarity on disordered surfaces. Diffusion constants were calculated using the mean-squared displacement of a molecule's center-of-mass projected onto the slab. Error bars are smaller than the data markers.

increase monotonically with polarity, the relationship was not linear, so D_{2d} was not exponential in the variance. The connection here is tenuous: our system is not one-dimensional, and the fluctuations in the potential are not necessarily Gaussian. The near-perfect exponential decay of the diffusion constant with polarity in Figure 4 is, however, striking.

For our results to have bearing on SF, the clustered structures must persist for time scales that are comparable to or longer than the time scale for SF. Because the herringbone well in the free energy surface is shallow, about 1 k_BT deep (Figure 1c), fluctuations away from the herringbone structure are facile. One might worry that the putative herringbone structure is nothing more than a fleeting fluctuation. We estimated the persistence time of the herringbone structures by measuring the time correlation function for a herringbone order parameter, which was unity when a given molecule was in a herringbone structure with at least one neighbor and zero otherwise.[75,76] Decay times of the time correlation function averaged poorly at our concentrations, but we estimate that herringbone structures survive on time scales from 10 to 100 ps. Estimates for the SF rate range from sub-ps to 100 ps;[7,21,39,77,78] therefore, it is likely that the herringbone structures identified here are stable on the time scale of SF. The lifetime of a cluster is longer: at least 1 ns. This is why REMD was necessary to achieve equilibrium.

Singlet fission could be the key to next-generation solar cells, but it is still difficult to establish design principles for cost-effective and robust devices. One of the most conceptually simple implementations of a SF device is a DSSC, but the functionality of a DSSC depends on the chromophore molecules aggregating in geometries that are suitable for SF. We found that a significant fraction of tetracene molecules on a surface did indeed self-assemble into herringbone structures at surface concentrations as small as a few percent of a monolayer. This result supports the hypothesis that herringbone structures in small aggregates give rise to the Davydov splitting seen in the absorption spectra of tetracene on silica at low surface coverage.[49] Further, the semiconductor surface can play an important role in both aggregation and SF; a recent study has found that SF in a DSSC requires a spacer layer on the semiconductor surface.[5] This layer could introduce a polar surface and allow for experimental tuning of the polarity. We found that when the surface was

DOI: 10.1021/acs.jpclett.5b00141
J. Phys. Chem. Lett. 2015, 6, 1209−1215

microscopically polar, the roughness in the potential between the molecules and the surface let the molecules adhere to pockets on the surface more strongly, resulting in less clustering, smaller clusters, and fewer molecules in herringbone structures. When the surface was macroscopically polar, the roughness in the potential disappeared, and surprisingly, the polarity did *not* affect clustering or herringbone formation statistics. The role of polarity is therefore subtle, and our results run counter to the expectation that clustering statistics arise from a microscopic version of phase separation, where nonpolar acene molecules form clusters as they retreat from a polar surface. Though our simulation results apply to tetracene, it is likely that the qualitative conclusions drawn here apply to other acene molecules that engage in singlet fission, like pentacene.

■ ASSOCIATED CONTENT

Supporting Information

Simulation details. This material is available free of charge via the Internet at http://pubs.acs.org.

■ AUTHOR INFORMATION

Corresponding Author

*E-mail: Joel.Eaves@Colorado.edu.

Notes

The authors declare no competing financial interest.

■ ACKNOWLEDGMENTS

We would like to thank Niels Damrauer for interesting discussions that prompted some of the work presented here. We would also like to acknowledge helpful conversations with Steve George. This work used the Janus supercomputer, which is supported by the National Science Foundation (Award Number CNS-0821794) and the University of Colorado Boulder. The Janus supercomputer is a joint effort of the University of Colorado Boulder, the University of Colorado Denver, and the National Center for Atmospheric Research. J.D.E. thanks the University of Colorado for generous startup funds and the Innovative Seed Grant program at CU. S.E.S. acknowledges support from the National Science Foundation Graduate Research Fellowship (Grant Number DGE-1144083).

■ REFERENCES

(1) Hanna, M. C.; Nozik, A. J. Solar Conversion Efficiency of Photovoltaic and Photoelectrolysis Cells with Carrier Multiplication Absorbers. *J. Appl. Phys.* **2006**, *100*, 074510−8.

(2) Shockley, W.; Queisser, H. J. Detailed Balance Limit of Efficiency of p-n Junction Solar Cells. *J. Appl. Phys.* **1961**, *32*, 510−519.

(3) O'Regan, B.; Grätzel, M. A Low-Cost, High-Efficiency Solar Cell Based on Dye-Sensitized Colloidal TiO_2 Films. *Nature* **1991**, *353*, 737−740.

(4) Teichen, P. E.; Eaves, J. D. A Microscopic Model of Singlet Fission. *J. Phys. Chem. B* **2012**, *116*, 11473−11481.

(5) Schrauben, J. N.; Zhao, Y.; Mercado, C.; Dron, P. I.; Ryerson, J. L.; Michl, J.; Zhu, K.; Johnson, J. C. Photocurrent Enhanced by Singlet Fission in a Dye-Sensitized Solar Cell. *ACS Appl. Mater. Interfaces* **2015**, *7*, 2286−2293.

(6) Smith, M. B.; Michl, J. Singlet Fission. *Chem. Rev.* **2010**, *110*, 6891−6936.

(7) Smith, M. B.; Michl, J. Recent Advances in Singlet Fission. *Annu. Rev. Phys. Chem.* **2013**, *64*, 361−386.

(8) Paci, I.; Johnson, J. C.; Chen, X.; Rana, G.; Popović, D.; David, D. E.; Nozik, A. J.; Ratner, M. A.; Michl, J. Singlet Fission for Dye-Sensitized Solar Cells: Can a Suitable Sensitizer Be Found? *J. Am. Chem. Soc.* **2006**, *128*, 16546−16553.

(9) Akdag, A.; Havlas, Z.; Michl, J. Search for a Small Chromophore with Efficient Singlet Fission: Biradicaloid Heterocycles. *J. Am. Chem. Soc.* **2012**, *134*, 14624−14631.

(10) Greyson, E. C.; Stepp, B. R.; Chen, X.; Schwerin, A. F.; Paci, I.; Smith, M. B.; Akdag, A.; Johnson, J. C.; Nozik, A. J.; Michl, J.; Ratner, M. A. Singlet Exciton Fission for Solar Cell Applications: Energy Aspects of Interchromophore Coupling. *J. Phys. Chem. B* **2009**, *114*, 14223−14232.

(11) Greyson, E. C.; Vura-Weis, J.; Michl, J.; Ratner, M. A. Maximizing Singlet Fission in Organic Dimers: Theoretical Investigation of Triplet Yield in the Regime of Localized Excitation and Fast Coherent Electron Transfer. *J. Phys. Chem. B* **2010**, *114*, 14168−14177.

(12) Johnson, J. C.; Nozik, A. J.; Michl, J. High Triplet Yield from Singlet Fission in a Thin Film of 1,3-Diphenylisobenzofuran. *J. Am. Chem. Soc.* **2010**, *132*, 16302−16303.

(13) Johnson, J. C.; Nozik, A. J.; Michl, J. The Role of Chromophore Coupling in Singlet Fission. *Acc. Chem. Res.* **2013**, *46*, 1290−1299.

(14) Roberts, S. T.; McAnally, R. E.; Mastron, J. N.; Webber, D. H.; Whited, M. T.; Brutchey, R. L.; Thompson, M. E.; Bradforth, S. E. Efficient Singlet Fission Discovered in a Disordered Acene Film. *J. Am. Chem. Soc.* **2012**, *134*, 6388−6400.

(15) Piland, G. B.; Burdett, J. J.; Kurunthu, D.; Bardeen, C. J. Magnetic Field Effects on Singlet Fission and Fluorescence Decay Dynamics in Amorphous Rubrene. *J. Phys. Chem. C* **2012**, *117*, 1224−1236.

(16) Wang, L.; Olivier, Y.; Prezhdo, O. V.; Beljonne, D. Maximizing Singlet Fission by Intermolecular Packing. *J. Phys. Chem. Lett.* **2014**, *5*, 3345−3353.

(17) Müller, A. M.; Avlasevich, Y. S.; Schoeller, W. W.; Müllen, K.; Bardeen, C. J. Exciton Fission and Fusion in Bis(tetracene) Molecules with Different Covalent Linker Structures. *J. Am. Chem. Soc.* **2007**, *129*, 14240−14250.

(18) Ma, L.; Zhang, K.; Kloc, C.; Sun, H.; Michel-Beyerle, M. E.; Gurzadyan, G. G. Singlet Fission in Rubrene Single Crystal: Direct Observation by Femtosecond Pump−Probe Spectroscopy. *Phys. Chem. Chem. Phys.* **2012**, *14*, 8307.

(19) Yost, S. R.; Lee, J.; Wilson, M. W. B.; Wu, T.; McMahon, D. P.; Parkhurst, R. R.; Thompson, N. J.; Congreve, D. N.; Rao, A.; Johnson, K.; Sfeir, M. Y.; Bawendi, M. G.; Swager, T. M.; Friend, R. H.; Baldo, M. A.; Van Voorhis, T. A Transferable Model for Singlet-Fission Kinetics. *Nat. Chem.* **2014**, *6*, 492−497.

(20) Liu, H.; Nichols, V. M.; Shen, L.; Jahanousz, S.; Chen, Y.; Hanson, K. M.; Bardeen, C. J.; Li, X. Synthesis and Photophysical Properties of a "Face-to-Face" Stacked Tetracene Dimer. *Phys. Chem. Chem. Phys.* **2015**, *17*, 6523−6531.

(21) Burdett, J. J.; Mueller, A. M.; Gosztola, D.; Bardeen, C. J. Excited State Dynamics in Solid and Monomeric Tetracene: The Roles of Superradiance and Exciton Fission. *J. Chem. Phys.* **2010**, *133*, 144506.

(22) Ryerson, J. L.; Schrauben, J. N.; Ferguson, A. J.; Sahoo, S. C.; Naumov, P.; Havlas, Z.; Michl, J.; Nozik, A. J.; Johnson, J. C. Two Thin Film Polymorphs of the Singlet Fission Compound 1,3-Diphenylisobenzofuran. *J. Phys. Chem. C* **2014**, *118*, 12121−12132.

(23) Lee, J.; Jadhav, P.; Baldo, M. A. High Efficiency Organic Multilayer Photodetectors Based on Singlet Exciton Fission. *Appl. Phys. Lett.* **2009**, *95*, 033301.

(24) Marciniak, H.; Fiebig, M.; Huth, M.; Schiefer, S.; Nickel, B.; Selmaier, F.; Lochbrunner, S. Ultrafast Exciton Relaxation in Microcrystalline Pentacene Films. *Phys. Rev. Lett.* **2007**, *99*, 176402.

(25) Kuhlman, T. S.; Kongsted, J.; Mikkelsen, K. V.; Møller, K. B.; Sølling, T. I. Interpretation of the Ultrafast Photoinduced Processes in Pentacene Thin Films. *J. Am. Chem. Soc.* **2010**, *132*, 3431−3439.

(26) Havenith, R. W. A.; de Gier, H. D.; Broer, R. Explorative Computational Study of the Singlet Fission Process. *Mol. Phys.* **2012**, *110*, 2445−2454.

(27) Zimmerman, P. M.; Bell, F.; Casanova, D.; Head-Gordon, M. Mechanism for Singlet Fission in Pentacene and Tetracene: From Single Exciton to Two Triplets. *J. Am. Chem. Soc.* **2011**, *133*, 19944−19952.

(28) Ramanan, C.; Smeigh, A. L.; Anthony, J. E.; Marks, T. J.; Wasielewski, M. R. Competition between Singlet Fission and Charge Separation in Solution-Processed Blend Films of 6,13-Bis(triisopropylsilylethynyl)pentacene with Sterically-Encumbered Pery-

DOI: 10.1021/acs.jpclett.5b00141
J. Phys. Chem. Lett. 2015, 6, 1209−1215

lene-3,4:9,10-bis(dicarboximide)s. *J. Am. Chem. Soc.* **2011**, *134*, 386−397.
(29) Eaton, S. W.; Shoer, L. E.; Karlen, S. D.; Dyar, S. M.; Margulies, E. A.; Veldkamp, B. S.; Ramanan, C.; Hartzler, D. A.; Savikhin, S.; Marks, T. J.; Wasielewski, M. R. Singlet Exciton Fission in Polycrystalline Thin Films of a Slip-Stacked Perylenediimide. *J. Am. Chem. Soc.* **2013**, *135*, 14701−14712.
(30) Müller, A. M.; Avlasevich, Y. S.; Müllen, K.; Bardeen, C. J. Evidence for Exciton Fission and Fusion in a Covalently Linked Tetracene Dimer. *Chem. Phys. Lett.* **2006**, *421*, 518−522.
(31) Quarti, C.; Fazzi, D.; Del Zoppo, M. A Computational Investigation on Singlet and Triplet Exciton Couplings in Acene Molecular Crystals. *Phys. Chem. Chem. Phys.* **2011**, *13*, 18615.
(32) Marciniak, H.; Pugliesi, I.; Nickel, B.; Lochbrunner, S. Ultrafast Singlet and Triplet Dynamics in Microcrystalline Pentacene Films. *Phys. Rev. B* **2009**, *79*, 235318.
(33) Johnson, J. C.; Akdag, A.; Zamadar, M.; Chen, X.; Schwerin, A. F.; Paci, I.; Smith, M. B.; Havlas, Z.; Miller, J. R.; Ratner, M. A.; Nozik, A. J.; Michl, J. Toward Designed Singlet Fission: Solution Photophysics of Two Indirectly Coupled Covalent Dimers of 1,3-Diphenylisobenzofuran. *J. Phys. Chem. B* **2013**, *117*, 4680−4695.
(34) Michl, J.; Nozik, A. J.; Chen, X.; Johnson, J. C.; Rana, G.; Akdag, A.; Schwerin, A. F. Toward Singlet Fission for Excitonic Solar Cells. *Proc. SPIE* **2007**, *6656*, 66560E.
(35) Schwob, H. P.; Williams, D. F. Charge Transfer Exciton Fission in Anthracene Crystals. *J. Chem. Phys.* **1973**, *58*, 1542−1547.
(36) Ryasnyanskiy, A.; Biaggio, I. Triplet Exciton Dynamics in Rubrene Single Crystals. *Phys. Rev. B: Condens. Matter* **2011**, *84*, 193203.
(37) Najafov, H.; Lee, B.; Zhou, Q.; Feldman, L. C.; Podzorov, V. Observation of Long-Range Exciton Diffusion in Highly Ordered Organic Semiconductors. *Nat. Mater.* **2010**, *9*, 938−943.
(38) Chen, Y.; Lee, B.; Fu, D.; Podzorov, V. The Origin of a 650 nm Photoluminescence Band in Rubrene. *Adv. Mater.* **2011**, *23*, 5370−5375.
(39) Burdett, J. J.; Gosztola, D.; Bardeen, C. J. The Dependence of Singlet Exciton Relaxation on Excitation Density and Temperature in Polycrystalline Tetracene Thin Films: Kinetic Evidence for a Dark Intermediate State and Implications for Singlet Fission. *J. Chem. Phys.* **2011**, *135*, 214508.
(40) Berkelbach, T. C.; Hybertsen, M. S.; Reichman, D. R. Microscopic Theory of Singlet Exciton Fission. I. General Formulation. *J. Chem. Phys.* **2013**, *138*, 114102.
(41) Berkelbach, T. C.; Hybertsen, M. S.; Reichman, D. R. Microscopic Theory of Singlet Exciton Fission. II. Application to Pentacene Dimers and the Role of Superexchange. *J. Chem. Phys.* **2013**, *138*, 114103.
(42) Berkelbach, T. C.; Hybertsen, M. S.; Reichman, D. R. Microscopic Theory of Singlet Exciton Fission. III. Crystalline Pentacene. *J. Chem. Phys.* **2014**, *141*, 074705.
(43) Schwerin, A. F.; Johnson, J. C.; Smith, M. B.; Sreearunothai, P.; Popović, D.; Černý, J.; Havlas, Z.; Paci, I.; Akdag, A.; MacLeod, M. K.; Chen, X.; David, D. E.; Ratner, M. A.; Miller, J. R.; Nozik, A. J.; Michl, J. Toward Designed Singlet Fission: Electronic States and Photophysics of 1,3-Diphenylisobenzofuran. *J. Phys. Chem. A* **2009**, *114*, 1457−1473.
(44) Renaud, N.; Sherratt, P. A.; Ratner, M. A. Mapping the Relation between Stacking Geometries and Singlet Fission Yield in a Class of Organic Crystals. *J. Phys. Chem. Lett.* **2013**, *4*, 1065−1069.
(45) Feng, X.; Luzanov, A. V.; Krylov, A. I. Fission of Entangled Spins: An Electronic Structure Perspective. *J. Phys. Chem. Lett.* **2013**, *4*, 3845−3852.
(46) Anthony, J. E. The Larger Acenes: Versatile Organic Semiconductors. *Angew. Chem., Int. Ed.* **2008**, *47*, 452−483.
(47) Anthony, J. E.; Eaton, D. L.; Parkin, S. R. A Road Map to Stable, Soluble, Easily Crystallized Pentacene Derivatives. *Org. Lett.* **2001**, *4*, 15−18.
(48) Maly, K. E. Acenes vs N-Heteroacenes: The Effect of N-Substitution on the Structural Features of Crystals of Polycyclic Aromatic Hydrocarbons. *Cryst. Growth Des.* **2011**, *11*, 5628−5633.
(49) Dabestani, R.; Nelson, M.; Sigman, M. E. Photochemistry of Tetracene Adsorbed on Dry Silica: Products and Mechanism. *Photochem. Photobiol.* **1996**, *64*, 80−86.
(50) Alguire, E. C.; Subotnik, J. E.; Damrauer, N. H. Exploring Non-Condon Effects in a Covalent Tetracene Dimer: How Important Are Vibrations in Determining the Electronic Coupling for Singlet Fission? *J. Phys. Chem. A* **2014**, *119*, 299−311.
(51) Walker, B. J.; Musser, A. J.; Beljonne, D.; Friend, R. H. Singlet Exciton Fission in Solution. *Nat. Chem.* **2013**, *5*, 1019−1024.
(52) Willard, A. P.; Chandler, D. Coarse-Grained Modeling of the Interface between Water and Heterogeneous Surfaces. *Faraday Discuss.* **2009**, *141*, 209−220.
(53) Willard, A. P.; Reed, S. K.; Madden, P. A.; Chandler, D. Water at an Electrochemical Interface—A Simulation Study. *Faraday Discuss.* **2009**, *141*, 423−441.
(54) Chandler, D. Interfaces and the Driving Force of Hydrophobic Assembly. *Nature* **2005**, *437*, 640−647.
(55) Willard, A. P.; Chandler, D. The Molecular Structure of the Interface between Water and a Hydrophobic Substrate Is Liquid-Vapor Like. *J. Chem. Phys.* **2014**, *141*, 18C519.
(56) Hagfeldt, A.; Boschloo, G.; Sun, L.; Kloo, L.; Pettersson, H. Dye-Sensitized Solar Cells. *Chem. Rev.* **2010**, *110*, 6595−6663.
(57) Hair, M. L. Hydroxyl Groups on Silica Surface. *J. Non-Cryst. Solids* **1975**, *19*, 299−309.
(58) Diebold, U. The Surface Science of Titanium Dioxide. *Surf. Sci. Rep.* **2003**, *48*, 53−229.
(59) Hoex, B.; Schmidt, J.; Pohl, P.; Sanden, M. C. M. v. d.; Kessels, W. M. M. Silicon Surface Passivation by Atomic Layer Deposited Al_2O_3. *J. Appl. Phys.* **2008**, *104*, 044903.
(60) Kroemer, H. Nobel Lecture: Quasielectric Fields and Band Offsets: Teaching Electrons New Tricks. *Rev. Mod. Phys.* **2001**, *73*, 783−793.
(61) Sweeney, M. C.; Eaves, J. D. Carrier Transport in Heterojunction Nanocrystals under Strain. *J. Phys. Chem. Lett.* **2011**, *3*, 791−795.
(62) Noguera, C. Polar Oxide Surfaces. *J. Phys.: Condens. Matter* **2000**, *12*, R367.
(63) Mayo, S. L.; Olafson, B. D.; Goddard, W. A. DREIDING: A Generic Force Field for Molecular Simulations. *J. Phys. Chem.* **1990**, *94*, 8897−8909.
(64) Mattheus, C. C.; de Wijs, G. A.; de Groot, R. A.; Palstra, T. T. M. Modeling the Polymorphism of Pentacene. *J. Am. Chem. Soc.* **2003**, *125*, 6323−6330.
(65) Sugita, Y.; Okamoto, Y. Replica-Exchange Molecular Dynamics Method for Protein Folding. *Chem. Phys. Lett.* **1999**, *314*, 141−151.
(66) Plimpton, S. Fast Parallel Algorithms for Short-Range Molecular Dynamics. *J. Comput. Phys.* **1995**, *117*, 1−19.
(67) Humphrey, W.; Dalke, A.; Schulten, K. VMD — Visual Molecular Dynamics. *J. Mol. Graphics* **1996**, *14*, 33−38.
(68) Stone, J. *An Efficient Library for Parallel Ray Tracing and Animation*; Computer Science Department, University of Missouri-Rolla: Rolla, MO, 1998.
(69) Chandler, D. *Introduction to Modern Statistical Mechanics*, 1st ed.; Oxford University Press: New York, 1987.
(70) Eaves, J. D.; Tokmakoff, A.; Geissler, P. L. Electric Field Fluctuations Drive Vibrational Dephasing in Water. *J. Phys. Chem. A* **2005**, *109*, 9424−9436.
(71) Campbell, R. B.; Robertson, J. M.; Trotter, J. The Crystal Structure of Hexacene, and a Revision of the Crystallographic Data for Tetracene. *Acta Crystallogr.* **1962**, *15*, 289−290.
(72) Bouchaud, J.-P.; Georges, A. Anomalous Diffusion in Disordered Media: Statistical Mechanisms, Models and Physical Applications. *Phys. Rep.* **1990**, *195*, 127−293.
(73) Banerjee, S.; Biswas, R.; Seki, K.; Bagchi, B. Diffusion on a Rugged Energy Landscape with Spatial Correlations. *J. Chem. Phys.* **2014**, *141*, 124105.
(74) Zwanzig, R. Diffusion in a Rough Potential. *Proc. Natl. Acad. Sci. U.S.A.* **1988**, *85*, 2029−2030.

DOI: 10.1021/acs.jpclett.5b00141
J. Phys. Chem. Lett. 2015, 6, 1209−1215

(75) Bennett, C. H. Exact Defect Calculations in Model Substances. In *Diffusion in Solids: Recent Developments*, Nowick, A. S., Burton, J. J., Eds.; Academic Press: New York, 1975; pp 73−113.
(76) Chandler, D. Statistical Mechanics of Isomerization Dynamics in Liquids and the Transition State Approximation. *J. Chem. Phys.* **1978**, *68*, 2959−2970.
(77) Chan, W.-L.; Ligges, M.; Jailaubekov, A.; Kaake, L.; Miaja-Avila, L.; Zhu, X.-Y. Observing the Multiexciton State in Singlet Fission and Ensuing Ultrafast Multielectron Transfer. *Science* **2011**, *334*, 1541−1545.
(78) Burdett, J. J.; Bardeen, C. J. The Dynamics of Singlet Fission in Crystalline Tetracene and Covalent Analogs. *Acc. Chem. Res.* **2013**, *46*, 1312−1320.

DOI: 10.1021/acs.jpclett.5b00141
J. Phys. Chem. Lett. 2015, 6, 1209−1215